THE JOURNAL OF PHYSICAL CHEMISTRY C

Article

pubs.acs.org/JPCC

Solvation and Dynamics of Lithium Ions in Carbonate-Based Electrolytes during Cycling Followed by Operando Infrared Spectroscopy: The Example of $NiSb_2$, a Typical Negative Conversion-Type Electrode Material for Lithium Batteries

Cyril Marino,[†] Athmane Boulaoued,[†,‡] Julien Fullenwarth,[†] David Maurin,[§] Nicolas Louvain,[†,∥] Jean-Louis Bantignies,[§] Lorenzo Stievano,[†,‡,∥] and Laure Monconduit*[,†,‡,∥]

[†]Institut Charles Gerhardt Montpellier, CNRS UMR 5253, Université Montpellier, 34095 Montpellier, France

[‡]Alistore European Research Institute (3104 CNRS), Université de Picardie Jules Verne, 33 rue Saint Leu, 80039 Amiens, France

[§]Laboratoire Charles Coulomb UMR 5221 CNRS, Université Montpellier 2, 34095 Montpellier, France

[∥]Réseau sur le Stockage Electrochimique de l'Energie (RS2E), CNRS FR 3459, 33 Rue Saint Leu, 80039 Amiens, France

Supporting Information

ABSTRACT: Conversion-type electrode materials show extremely interesting performance in terms of capacity, which is however usually associated with bad Coulombic efficiency. The latter is mainly the consequence of the relentless evolution of solid electrolyte interphase (SEI) formed and/or dissolved during conversion/back-conversion reactions on the continuously reshaping active material surface. The thorough comprehension of the dynamic processes occurring during cycling in a working electrochemical cell, such as solvation/desolvation of ionic species and formation/dissolution of the SEI at the electrode/electrolyte interface, is thus of utmost relevance in the study of electrochemical mechanism and performance of conversion-type electrode materials. Operando Fourier transform infrared (FTIR) spectroscopy, one of the methods of choice for the study of such phenomena, was applied to study the dynamic interfacial properties of $NiSb_2$, a representative intermetallic conversion-type electrode material for Li batteries, during cycling in the presence of a commercial electrolyte based on $LiPF_6$ dissolved in a mixture of ethylene carbonate (EC) and dimethyl carbonate (DMC). Using a specifically developed in situ ATR-IR electrochemical cell, it was possible to correlate the electrochemical processes to the ratio between solvent molecules associated with Li^+ ions and free solvent molecules and thus to follow the dynamic evolution of the concentration of lithium in the electrolyte during cycling.

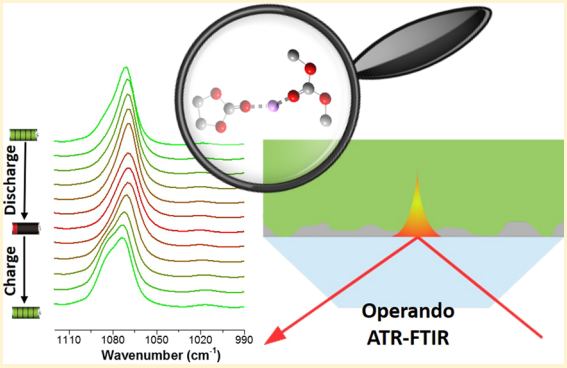

1. INTRODUCTION

Over recent years, the world has witnessed considerable interest in Li-ion batteries (LIB) as a consequence of their broad and growing use in many vital applications such as portable devices, vehicles, satellites, etc. Both performance and safety issues on LIB are closely related to interfacial processes, such as diffusion of electrolyte species, solvation/desolvation of lithium ions, decomposition of the electrolyte, and formation of the solid electrolyte interphase (SEI).[1,2] The crucial function of a stable SEI is preventing further chemical reactions between the electrode and the electrolyte, while allowing lithium ions conduction to and from the electrode. Commonly SEI is formed by the buildup of reduction products of carbonate-based electrolyte on negative electrodes such as silicon, tin, and graphite.[3,4] In order to unravel the chemical and physical properties of the SEI, considerable endeavors led to highlighting its key role in ensuring high Coulombic efficiency,[5] cycle life,[5,6] and safety.[6,7] As the continuous evolution of the SEI (deposition/dissolution) in batteries during cycling goes together with other concomitant evolving electrochemical processes (lithiation/delithiation of electrode materials, solvation/desolvation of electrolyte species, etc.), the possibility of characterizing the dynamics of these phenomena within a working cell is of great pertinence. For this reason, many research works have been concerned with the investigation of battery materials by many various in situ/operando experiments (transmission electron microscopy,[8−10] NMR spectroscopy,[11,12] X-ray absorption spectroscopy,[13,14] Raman spectroscopy,[15,16] Fourier transform infrared spectroscopy (FTIR),[2,17,18] etc.). Among these techniques, FTIR spectroscopy has been used to obtain vital information on the molecular structure of the electrode/electrolyte interface. Historically, the pioneering

Received: July 7, 2017
Revised: October 18, 2017
Published: November 13, 2017

DOI: 10.1021/acs.jpcc.7b06685
J. Phys. Chem. C 2017, 121, 26598−26606

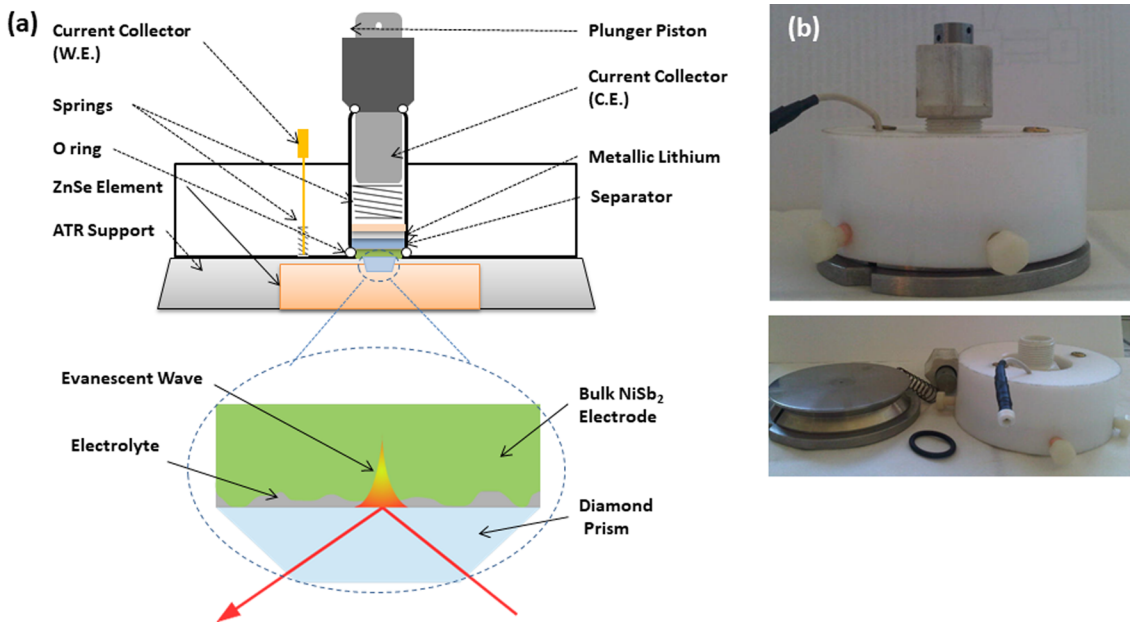

Figure 1. (a) Scheme of the in situ electrochemical cell used for the operando ATR-FTIR experiment and (b) pictures of the different components of the in situ cell.

FTIR works on the electrolyte/electrode interface by Bewick and Pons[19,20] have been a milestone in the development of FTIR interfacial analysis. Later, many groups have used FTIR, either in operando mode to follow the electrochemical reduction−oxidation processes, or ex situ after cycling to get better insight on the final products of electrolyte degradation. An interesting investigation by operando FTIR spectroscopy by Li et al.[21,22] revealed the processes of lithiation/delithiation and electrolyte decomposition on Sn-based electrodes. Similarly, the chemistry developed on a number of electrode surfaces has been widely investigated, including silicon,[23,24] carbon,[25−28] as well as noble[29,30] and non-noble metals.[17,31]

Traditional electrolytes for LIB often contain lithium hexafluorophosphate ($LiPF_6$) dissolved in a mixture of linear and cyclic organic carbonates. Each one of these compounds has its virtues: $LiPF_6$ associates distinctively several suitable properties, such as temperature range of operation, passivation, and conductivity.[32,33] Cyclic carbonates such as ethylene carbonate (EC) produce high salt dissociation, in contrast with their linear counterparts, e.g., dimethyl carbonate (DMC) and ethyl methyl carbonate (EMC), which are not as good in dissociating lithium salts, but typically retain a low viscosity whereby ion transport is enhanced, especially at low temperatures.[34] The composition of the electrolyte and the deriving evolution of solvated species during cycling is crucial for the formation of a stable SEI; in particular, the coordination of solvent molecules to Li^+ ions induces a higher polarization and, hence, a higher affinity to reduction compared to free solvent. As a result, the solvation shell of Li^+ will contribute to the composition of the SEI by affecting the preferential reduction potential of solvents.[34] It follows that the investigation of salt dissociation and Li^+ solvation shell in the electrolyte may help to understand the properties and the performance of a LIB electrode. That is what prompted many research groups to undertake numerous theoretical[34−38] and experimental[34,36] studies on the Li^+ solvation structure. For example, Brooksby et al.[39] studied the concentration dependence of the solvation of Li and Na perchlorates by propylene carbonate (PC) and indicated from factor analysis of IR data that Li^+ and ClO_4^- are ion paired to PC whereas (at comparable concentration) Na^+ and ClO_4^- are not. Borodin at al.[34] studied by molecular dynamics and DFT the salt concentration dependence of Li^+ solvation shell, showing a preferential coordination of Li^+ to EC over DMC at low salt concentrations, in contrast to high concentrations where a slight preference for DMC over EC is observed. Moreover, they compared the calculated Li^+ solvation number to the value deduced from NMR, FTIR, and Raman spectroscopy and associated the observed discrepancies in the underestimation of Li^+ bonding to the noncarbonyl oxygen. Recently, Kuroda et al.[40] studied the solvation of Li^+ in carbonate solvents (EC, PC, DMC, and DEC) by time-resolved FTIR, identifying tetrahedral complexes of Li^+ bound to solvent molecules.

The above-mentioned studies bear on the solute−solvent interaction as a function of concentration, ion nature, and solvents. However, only few of them associate Li^+ solvation to battery state (i.e., are performed operando). Therefore, a direct correlation of Li^+ solvation to the electrochemical processes occurring during cycling is still lacking.

In this paper, we aimed to shed some light on the interfacial phenomena at the electrode/electrolyte interface of a $NiSb_2$-based electrode using operando ATR-FTIR spectroscopy. $NiSb_2$ is a representative conversion-type negative electrode material with high theoretical specific capacity (532 mAh g^{-1}). Conversion reactions, recently reviewed by Cabana et al.,[41] occur between lithium and a binary compound containing a transition metal (here Ni) and a group p element (here Sb), according to the equation

$$NiSb_2 + 0.5Li \rightarrow Li_xNiSb_2 \quad (x \approx 0.5)$$

$$NiSb_2 + 6Li \leftrightarrows Ni + 2Li_3Sb$$

The first reaction corresponds to the insertion of Li in pristine bulk $NiSb_2$ and is detectable only at the beginning of the first discharge. The second reaction corresponds to the reversible conversion leading to a complete structural

DOI: 10.1021/acs.jpcc.7b06685
J. Phys. Chem. C 2017, 121, 26598−26606

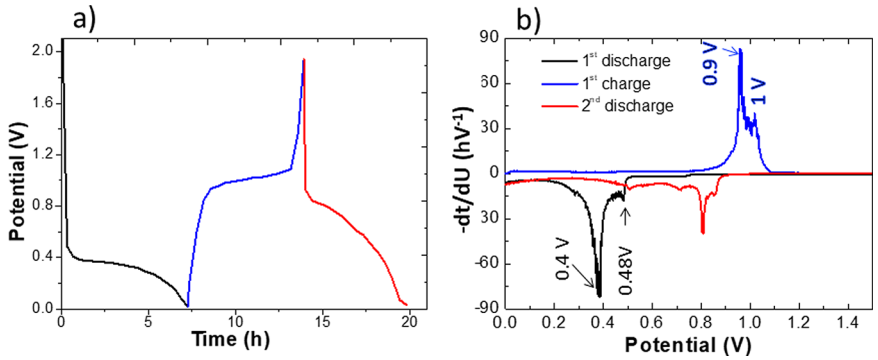

Figure 2. Galvanostatic potential curve (a) and its derivative (b), obtained during the operando FTIR experiment on $NiSb_2$ electrode cycled at 1C rate with 1 M $LiPF_6$ in EC:DMC (1:1) + 2%$_{vol}$ VC electrolyte.

rearrangement of pristine $NiSb_2$ and the formation of new phases.

Conversion materials allow reversible capacities exceeding that of current commercial lithium-ion batteries based on graphite and $LiCoO_2$. Therefore, they are looked with interest as a possible alternative for the future development of high energy storage devices needing a long cycling life, with applications extending from laptop computers to cell phones and electric vehicles. Even though both conversion mechanism and cycle life of $NiSb_2$ have been elucidated in previous studies,[42−45] the related electrolyte solvation dynamics and SEI formation processes have not yet been addressed. This new knowledge was thus obtained through a specifically developed FTIR in situ cell. The operando FTIR experiment consists of following quantitatively the dynamics of Li^+ ion solvation/desolvation within the solvent during electrochemical cycling. We were able to scrutinize the modification of molecular vibrations and to correlate the evolution of the different electrolyte species to the evolving electrochemical processes.

2. MATERIALS AND METHODS

2.1. ATR-FTIR Experiment. The specifically developed in situ electrochemical cell used for the ATR-FTIR experiments is shown in Figure 1. The ATR module consists of a single reflection diamond waveguide with a diameter of 5 mm supported on a ZnSe substrate casted on a cylindrical stainless steel support. The $NiSb_2$ self-standing working electrode has a diameter of 12 mm and is pressed against the diamond probe, so that the sampling surface of the diamond is completely covered by the electrode and the surrounding steel support serves as a current collector. The upper Teflon parts of the cell contain a Teflon Swagelok cell, with a plunger pressing on a spring, on top of which a copper disc supporting the Li metal counter electrode is mounted. The two electrodes are kept apart by a Whatman glass fiber separator, and the spring pushes the cell toward the diamond waveguide, ensuring an optimized optical contact between the $NiSb_2$ electrode and the diamond during the operando FTIR experiments. Furthermore, rubber O-rings are used to maintain a waterproof and airtight seal between the different parts of the cell. Once assembled, the cell is placed in the spectrometer between optical elements focusing the infrared (IR) beam to the diamond crystal with an incidence of 45° relative to interface.

Operando FTIR experiments in the middle infrared range (4000−400 cm^{-1}) were carried out in attenuated total reflectance (ATR) mode on a Bruker IFS 66 V spectrometer under argon. A deuterated, L-alanine doped triglycine sulfate (DLaTGS) thermal detector, a KBr beam splitter, and a blackbody source were used. The spectral resolution was 2 cm^{-1}, and 128 interferograms were coadded for each spectrum. During the first discharge, spectra are recorded every 2 min and in the following every 5 min. Spectra are represented as a function of the ATR intensity I ($I = \log_{10}(R_0/R)$, where R_0 is the ATR intensity after reflection at the diamond/air interface and R is the ATR intensity after reflection at the diamond/electrode interface). Spectra are given without any baseline subtraction and penetration depth normalization.

The probed thickness of the studied electrode is defined by the penetration depth of the evanescent wave, which is defined as the distance required for the electric field amplitude to fall to e^{-1} of its value at the surface and is further defined by

$$d_e = \frac{\lambda}{2\pi\sqrt{d^2 \sin\theta^2 - s^2}}$$

with λ being the wavelength of the beam, θ is the incidence angle, and d and s are the refractive angles of diamond and of the sample. Considering the wavelength in the middle infrared (typically 3−20 μm) and the optical parameters of the ATR module ($\theta = 45°$ and $d = 2.4$), the penetration depth of the IR beam is approximately the same order of magnitude as the wavelength (about 10 μm) and therefore cannot be considered simply as a probe of the external surface of the electrode.

2.2. Electrode Elaboration. A self-supported electrode was prepared using carboxymethyl cellulose (CMC; DS = 0.7, M_w = 250 000 Aldrich) as binder and carbon black (CB; Y50A, BET primary particle size 20−60 nm, primary aggregate size 100 nm, 70 m^2 g^{-1}, DBP oil absorption 640 mL/100g, SN2A) as conductive additive. $NiSb_2$ powder (synthesis described in detail in previous papers[42,45]), CMC (carboxymethyl cellulose), and CB (carbon black; 56/22/22% weight ratio) were introduced with deionized water into an agate jar containing 4 × 4 mm diameter agate balls. A Fritsch Pulverisette 7 was used to mill the mixture at 500 rpm for 1 h. The slurry was tape casted onto a 22 μm thick copper foil at 400 μm thickness. The obtained electrode was oven-dried for 30 min at 70 °C, and no adhesion on copper foil is observed. Finally, the self-supported electrode was dried under vacuum for 30 min at 100 °C. The final thickness of the dried electrode is below 100 μm.

A half cell was assembled in the glovebox using the $NiSb_2$ composite as the working electrode, a porous glass-fiber paper (Whatman) as the separator, and metallic lithium as the counter electrode. The used electrolyte was a 1 M solution of $LiPF_6$ in ethylene carbonate−dimethyl carbonate (EC−DMC) 1:1 containing 2%$_{vol}$ vinylene carbonate (VC) as additive.

DOI: 10.1021/acs.jpcc.7b06685
J. Phys. Chem. C 2017, 121, 26598−26606

Galvanostatic cycling was performed at 22 °C in argon and monitored by a VMP system (Bio-Logic) from 0.02 to 2 V vs Li^0/Li^+. The electrochemical tests were conducted at C rate, defined as the reaction of one mole of Li^+ per mol of $NiSb_2$ in 1 h. In this way, the full discharge corresponding to the theoretical reaction of 6 Li per mol of $NiSb_2$ to form 2 mol of Li_3Sb is expected to last 6 h.

3. RESULTS AND DISCUSSION

3.1. Electrochemical Properties. The electrochemical curves obtained during the operando FTIR experiment are shown in Figure 2. Previous studies on $NiSb_2$ report the same electrochemical behavior.[42,43] The Coulombic efficiency of 90% observed for the first discharge (Figure 2a) is due to the reduction of electrolyte species, which ensures the formation of a SEI layer. During the first discharge, the first peak at 0.48 V in the derivative curve is associated (Figure 2b) to the insertion of lithium in the structure of $NiSb_2$ to give Li_xNiSb_2 ($x \approx 0.5$) by a monophasic mechanism. Then, the resulting lithiated alloy undergoes a conversion into a mixture of Li_3Sb and Ni nanoparticles (peak around 0.4 V).

During the subsequent charge, the galvanostatic derivative curve is composed of two peaks at 0.95 and 1 V: the first peaks is associated with the back conversion from Ni and Li_3Sb to $NiSb_2$.[42] The less intense peak around 1 V is related to the formation of some metallic Sb, as demonstrated by previous Mössbauer studies, likely due to a nonstoichiometry in Sb in the nickel antimonide $NiSb_{2-x}$.[43] During the second discharge, the conversion of the obtained $NiSb_{2-x}$ and the lithiation of Sb take place (broad peak at about 0.8 V).

3.2. Operando ATR-FTIR Results. The operando FTIR investigation is focused on the quantitative study of the dynamics of the Li^+ solvation process in the electrolyte solution at the electrode/electrolyte interface. Li^+ solvation is well-known to affect significantly the infrared absorption spectra.[2,21,22,32,39,40] Indeed, in such systems, the magnitude of the frequency shifts of a band is expected to be related to the charge-to-radius ratio of the solvated ion.[39,46,47] Moreover, it has been shown that a coordination interaction between Li^+ and the most electronegative oxygen of the EC (or DMC) is created, modifying the force constant of their intramolecular bonding.[21,22,2,38] Therefore, the variation in energy (red or blue shift) of the stretching vibration of solvent indicates a strong interaction (solvation) with Li^+. For example, the solvation of Li^+ by DMC causes both the weakening of νC═O, which prompts a red shift (from 1750 to 1725 cm^{-1}), and the strengthening of O−C−O binding which induces a blue shift (from 1275 to 1321 cm^{-1}).

The evolution of the in situ FTIR spectra of the $NiSb_2$ film electrode measured during electrochemical cycling is shown in Figure 3 for the first discharge and Figure S2−S3 for the subsequent cycles. All infrared features originate from the electrolyte mixture EC/DMC and $LiPF_6$. The band assignment based on literature,[22,27,32,36,48−51] as well as on solvent reference spectra (Figure S1) in the 800−2000 cm^{-1} range, is given in Table 1. The reference spectrum of the pristine electrolyte at OCV (approximately 2.5 V vs Li^+/Li) before starting the discharge is shown in Figure 3, and the subsequent FTIR spectra give insights about the electrochemical process during discharge/charge cycles (Figures 3, S1, and S2). We note that no significant signal from VC,[52] and from the solid $NiSb_2$ electrode, is detectable in the observed/measured IR frequencies range. The lack of signal from VC is probably due

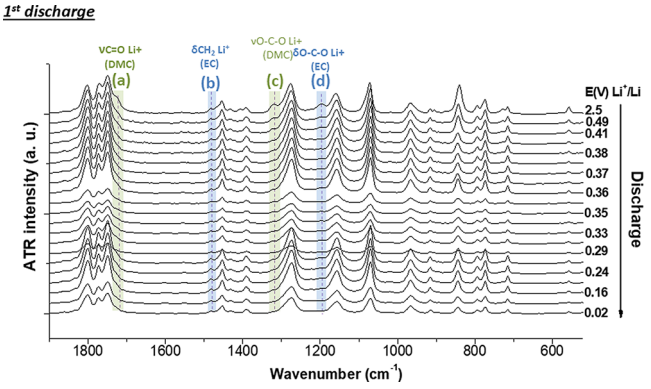

Figure 3. Operando IR spectra during the 1st discharge of $NiSb_2$ electrode at 1C rate with 1 M $LiPF_6$ in EC:DMC (1:1) + 2%$_{vol}$ VC electrolyte.

Table 1. FTIR Band Assignment of the 1 M $LiPF_6$ in EC/DMC (1:1), 2% VC Electrolyte[a]

wavenumber (cm^{-1})	band assignment	species of origin	refs
1800	νC═O	EC	22,27,36,51
1772	νC═O and νC═O Li^+	EC	22,27,50,51
1750	νC═O	DMC	22,27,36,49,50
1725	νC═O Li^+	DMC	22,36,49,50
1467	δCH_3 Li^+	DMC	22,50
1456	δCH_3	DMC	22,27,50
1407	δCH_2 Li^+	EC	22,50
1392	δCH_2	EC	22,27,50
1321	νO−C−O Li^+	DMC	22,50
1277	νO−C−O	DMC	22,50
1198	νO−C−O Li^+	EC	22,50
1155	νO−C−O	EC	22,27,50
1085	νC−O Li^+	EC	22,50
1069	νC−O	EC	22,50
840	νP−F	$LiPF_6$	32,49

[a] ν stands for stretching and δ for bending vibration.

to the starting low concentration of this species in the electrolyte. Our experimental conditions would not, in fact, allow the observation of the possible selective adsorption of VC at the surface of the carbon particles, recently observed by Peng et al. using sum-frequency generation spectroscopy.[53]

The bands at 1750, 1456, and 1277 cm^{-1} correspond to IR active modes of free DMC molecules, while free EC molecules show bands at 1800, 1772, 1407, 1155, and 1069 cm^{-1}. It is interesting to notice that the carbonyl region of EC consists of two contributions: the νC═O band at 1805 cm^{-1} is doubled at 1755 cm^{-1} due to Fermi resonance caused by the combination of the C═O stretching to overtones and totally symmetric combination tones in the same region.[36,51] The stretching band νP−F of $LiPF_6$ salt in its free state (nonsolubilized) expected to appear at 844 cm^{-1} is seen at 840 cm^{-1}, most probably as a consequence of solvation.[49] The bands of free solvent molecules $(EC/DMC)_{free}$ are consistently present during the cycling. The other bands, showing up as shoulders of the free vibrational features (marked in Figure 3 by a−d) are related to EC/DMC molecules solvating Li^+ $(EC/DMC)_{solv.}$; bands at (1725 cm^{-1}) and c (1321 cm^{-1}) correspond respectively to νC═O and νC−O of DMC_{solv}, while bands b (1407 cm^{-1}) and d (1198 cm^{-1}) correspond to δCH and νC−O of EC_{solv}. The νC═O band of EC_{solv} is not directly visible since it overlaps

DOI: 10.1021/acs.jpcc.7b06685
J. Phys. Chem. C 2017, 121, 26598−26606

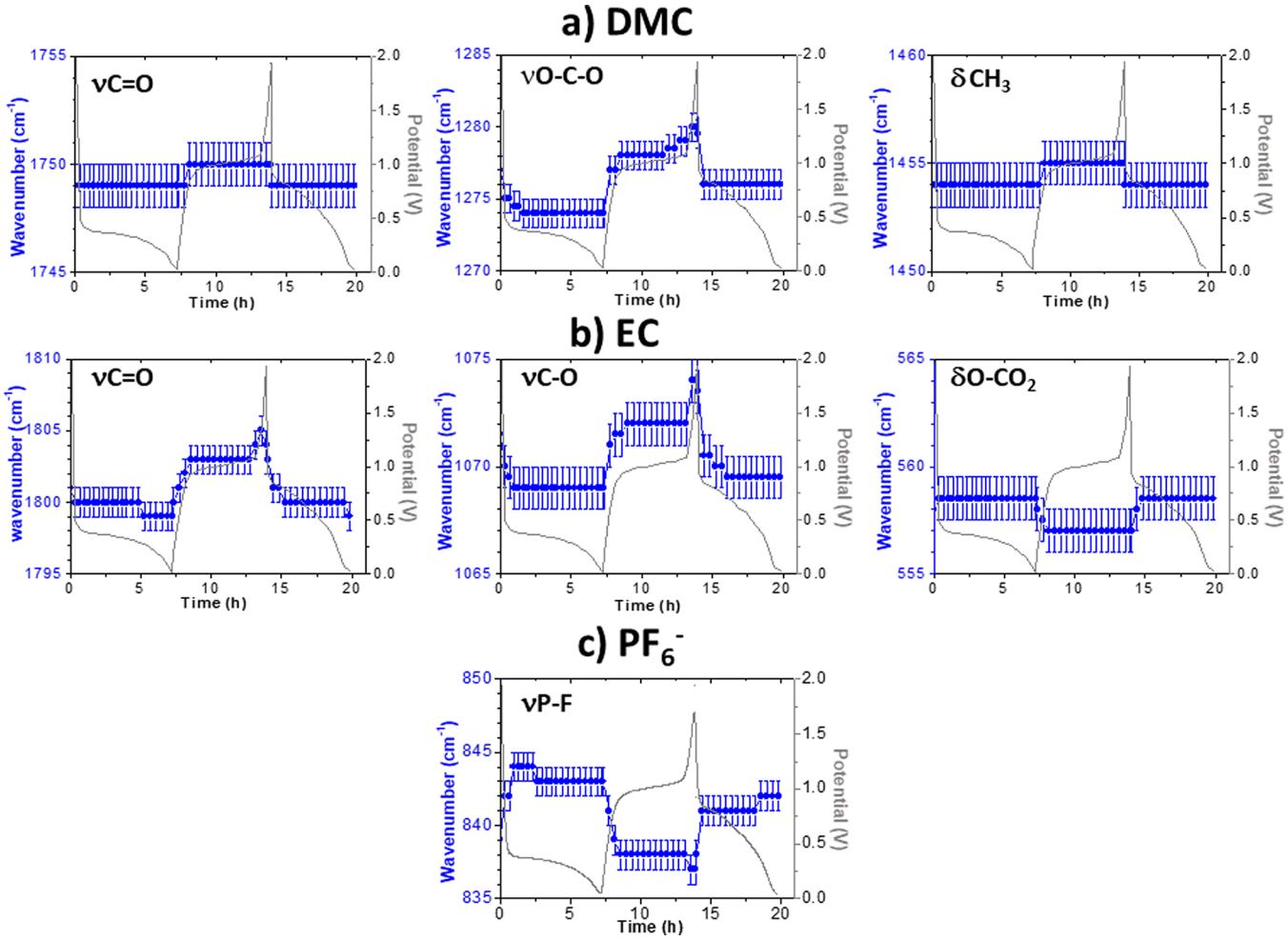

Figure 4. Evolution of peak position and voltage profile versus time during the electrochemical cycling for the bands of (a) DMC, (b) EC, and (c) PF_6^-.

with the Fermi resonance of EC_{free} at 1772 cm^{-1}, preventing any meaningful deconvolution of the peaks of EC_{free} and EC_{solv}.

During the first discharge, $(EC/DMC)_{solv}$ bands steadily decrease and tend to disappear at low potential. The reverse behavior is observed during the subsequent charge and reproduced upon a second discharge (see Figures S2 and S3). Upon discharging, $NiSb_2$ is transformed into Li_3Sb and the EC and DMC solvents undergo reduction processes below 1 V vs Li^+/Li. Concomitantly, at the interface, the concentration of $(EC/DMC)_{free}$ increases as $(EC/DMC)_{solv}$ decreases. The reverse process takes place upon the charge.

It is worth noting that during the first discharge, considerable decrease of the IR band intensities occurs between 0.36 and 0.35 V. The ATR intensity decrease depends on the band, while no new bands are detected. As the electrode does not contribute significantly to the IR spectrum in this frequency range, this phenomenon could be related either to a change in refraction index of the medium absorbing the evanescent IR wave (the penetration depth is inversely proportional to refractive indexes of material and waveguide) or to a decrease of the optical contact related to the morphological modifications. Interestingly, Villevieille et al.[54] also studied the same electrode/electrolyte system (see the Supporting Information, Figure S4) by operando acoustic emission, showing an important increase of the acoustic signal in the same potential range during the discharge. This behavior is in line with the occurring of important morphological modifications between the middle and the end of the conversion plateaus.

In the following sections, we will discuss the dynamics processes concerning the solvated Li^+ ions at the electrode/electrolyte interface throughout analysis of position and intensity of significant bands (νC═O, νC−O, and νP−F).

3.3. Discussion. *3.3.1. Frequency Band Behavior.* In Figure 4 both IR band frequencies and potential profile of the battery are plotted versus time during cycling. At first glance, one can notice that the wavenumbers of the bands are directly correlated to the state of charge of the battery.

In particular, the evolution of the bands of DMC and EC (Figures 4a,b and S5) during cycling is very similar and somehow follows the electrochemical potential. During the early stage of the first discharge (E > 0.3 V vs Li^+/Li), a weak but significant red shift of the νC═O and νC−O bands of free solvent species suggests increasing electrostatic interactions between ionic species in solution and $(DMC/EC)_{free}$ weakening the intramolecular bonding of free solvent species. This effect is observed before the setting of the conversion reaction and could be correlated to the formation of the SEI. In this case, the reaction of solvent molecules and possibly ionic species during SEI formation is expected to make up for Li^+ consumed by the electrochemical system. In the following part of the discharge, during the conversion reaction, peak positions

DOI: 10.1021/acs.jpcc.7b06685
J. Phys. Chem. C 2017, 121, 26598−26606

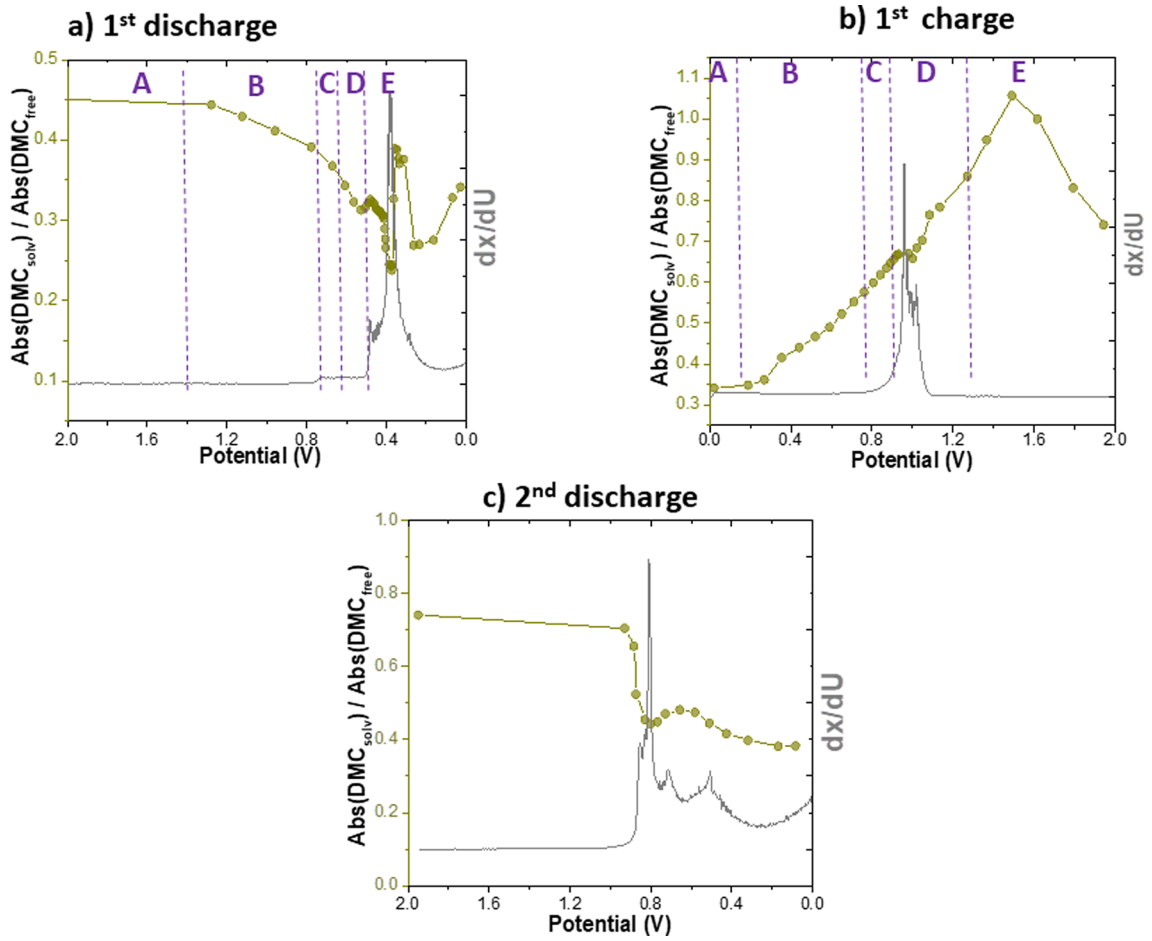

Figure 5. Evolution of absorbances ratio (DMC_{solv}/DMC_{free}) of $\nu C{=}O$ band with the corresponding galvanostatic derivative curve during the operando FTIR experiment.

are stable, suggesting the setting of a relatively constant concentration gradient at the interface while Li^+ reacts with $NiSb_2$, with the setting of a certain state of balance between $(EC/DMC)_{solv}$ and $(EC/DMC)_{free}$ molecules. This step highlights the vital role of concentration gradients at the electrode/electrolyte interface for the electrochemical system.

At the end of discharge, after the completion of the conversion of $NiSb_2$, the $\nu C{=}O$ band, especially the one around 1800 cm^{-1}, gradually shifts toward low frequencies, suggesting an increasing electrostatic interactions between Li^+ and $(DMC/EC)_{free}$, in line with a gradient of Li^+ concentration to compensate the continuing Li^+ consumption at low potentials due to the trapping of Li along the SEI formation. Upon charge, a steep increase of the EC/DMC band positions (blue shift) is observed at the beginning related to the inversion of the concentration gradient at the interface related to the release of Li^+. The band positions remain then constant during the rest of the back conversion, in line with the behavior observed during the first discharge. This observation clearly attests the reversibility of the solvation/desolvation process. Furthermore, the opposite shift behavior for $\nu P{-}F$ vibration (Figure 4c) relative to EC/DMC molecules testifies to the dissociation of $LiPF_6$ salt to Li^+ and PF_6^- during the discharge (blue shift of $\nu P{-}F$), associated with the consumption Li^+ by the system, and conversely during the charge (redshift of $\nu P{-}F$). The dependence of δCH_3 (DMC) and $\delta OCO2$ (EC) upon cycling on Figure 4 (see also Figure S5) suggest that not only the carbonyl groups experience the effect of the solvation process.

3.3.2. Band Intensities Behavior. The ratio of the peak intensity of the bands $\nu C{=}OLi^+$ of DMC_{solv} (1725 cm^{-1}) to $\nu C{=}O$ of DMC_{free} (1750 cm^{-1}) vs the potential during cycling are drawn in Figure 5 together with the derivative of the corresponding galvanostatic curve. The plotted results allow one to straightforwardly follow the lithiation/delithiation process at the electrode/electrolyte interface during cycling. It should be noted that the same analysis carried out on other bands of DMC and EC shows a very similar behavior.

During the first discharge (Figure 5a), several steps can be identified. First, in the region at high potential denominated (A), the ratio DMC_{solv}/DMC_{free} remains constant, meaning that there is no significant Li^+ consumption in the range 2.0−1.2 V. Then between 1.2 and 0.5 V (region B), the ratio decreases steadily concomitantly to a shift of the $\nu C{=}O$ bands of the solvent. This potential range matches the reduction of electrolyte components,[26] starting from the polymerization of VC,[31,55] followed by the reduction of EC and DMC to form the SEI (Li_2CO_3, CH_3OLi, $ROCO_2Li$, etc.).[31,56] Unfortunately, these products cannot be easily detected as their bands mostly overlapped with the prevailing bands of the electrolyte.[57]

Region C corresponds to the first peak of the galvanostatic derivative curve, which was attributed in previous works to the insertion of lithium in $NiSb_2$ to form Li_xNiSb_2 ($x \approx 0.5$).[42] In this region, the corresponding intensity ratio first increases

DOI: 10.1021/acs.jpcc.7b06685
J. Phys. Chem. C 2017, 121, 26598−26606

slightly then decreases. This could be due to an increase of DMC_{solv} at the interface between electrode and electrolyte as a consequence of the concentration gradient (Figure 4). Even though Tasaki et al.[58] showed that many degradation products including $ROCO_2Li$ are highly susceptible to solubilize in DMC and EC solvents, it is hardly conceivable to experience such partial solubilization of the just formed SEI before the onset of the conversion reaction. In any case, it is only after the starting of Li^+ insertion within the $NiSb_2$ matrix that the amount of solvated Li^+ (DMC_{solv}) is substantially reduced.

For zone D, corresponding to the following conversion of Li_xNiSb_2 to Li_3Sb and metallic Ni, the abrupt decrease of the absorbance ratio points to a strong decrease of DMC_{solv} which is likely connected to the massive reaction of Li^+ with the electrode (at ca. 0.415 V). At the maximum of the derivative curve, an anomalous behavior is observed; the ratio DMC_{solv}/DMC_{free} upturns suddenly. This response matches exactly the incident recorded during the operando experiment on the same systems reported by Villevieille et al.[54] Furthermore, Maier et al.[59] pointed out that this region corresponds in the case of conversion materials to a phase separation, which in our system should be associated with the conversion from $NiSb_2$ to Li_3Sb + Ni^0. Therefore, additional and "fresh" surfaces are formed in the electrode due to the phase separation or cracks of particles originating from the conversion reaction. Assuming that a possible induced change of refraction index of the medium does not sensibly affect the ratio DMC_{solv}/DMC_{free}, the sudden increase in DMC_{solv} molecules concentration could be explained by the wetting of the "fresh" surfaces with the electrolyte. In the following, the ratio decreases by increasing DMC_{free} molecules in agreement with Li^+ consumption by conversion reaction.

The end of discharge (zone E) is first characterized by a constant value of the absorbance ratio, followed by a steady increase at 0.15 V. However, one does expect no more faradaic reactions attributable to the conversion reaction in this potential range but rather the reaction of Li^+ with the carbon contained in the electrode. Besides, Gachot et al.[60] showed that, in conversion reactions at the very end of the discharge, a polymer gel forms at low potentials, composed of electrolyte degradation products not containing Li^+. Such reaction would be in line with the increase of the DMC_{solv}/DMC_{free} ratio. As for the operando experiment, it is possible that a balance between both phenomena (Li^+ insertion within C and gel creation) takes place and results in a concentration gradient of Li^+ more or less constant at the interface. It is only after the achievement of Li^+ reaction with carbon that the polymer gel formation would prevail and upset the balance.

During the beginning of the charge (Figure 5b, region A), the short stagnation of the absorbance ratio from 0.02 to 0.3 V indicates a very small modification of the species, showing that no faradaic nor nonfaradaic reaction takes place at the probed interface. Interestingly, the ratio increases then gradually (region B) but $NiSb_2$ is not supposed to be active at this potential range (see the derivative curve in Figure2b). Therefore, a rebalancing of Li^+ concentration can be expected since no electrochemical reaction is occurring. In fact, at the end of discharge, the interface is mainly composed of DMC_{free} molecules far from the equilibrium state observed at the beginning of the experiment. The possibility that Li^+ is released from the electrode because of the partial dissolution of the SEI and/or of the polymer gel formed at the end of the discharge exists but would be limited in terms of concentration.[61] The system then relaxes to reach a constant gradient of Li^+ concentration. After this increase, the back-conversion reaction is marked by a very minor modification of the ratio (region C), from the beginning to the maximum of the galvanostatic reaction peak, followed by a short and steep increase. This might be explained by a re-equilibration of the concentration gradient at the interface after the end of the release of Li^+. At a potential exceeding 1.2 V (zone D), the reaction is complete, and a rebalancing between Li^+ at the electrode interface (system relaxation) and SEI dissolution is supported by the upturn of the ratio with the same slope as in zone B. At 1.6 V, the ratio reaches a maximum for which $I_{Abs}(DMC_{solv}) \approx I_{Abs}(DMC_{free})$, but after this point, surprisingly (region E), the ratio drops with the same slope (in absolute value) as before the back-conversion reaction.

Finally, during the following second discharge, (cf. Figure 5c) a significant decrease of the ratio is observed once the conversion reaction starts (symbolized by the peak in the derivative curve). Unlike the first discharge, only a limited and smooth increase of the ratio is visible in the graph. The absence of the strong "earthquake" in further cycling was already supported by the acoustic experiment.[54] Therefore, our experiment strongly supports that dramatic changes happen during the first discharge for conversion materials with the nanostructuration of the electrode. For the following cycles, the proximity of the phases involved in the conversion reaction created by the nanostructuration during the first cycle[62] allows an easier and smooth reaction. The ratio then keeps a constant value down to the end of the discharge.

4. CONCLUSIONS

A conversion reaction holds the promise of higher energy density Li-ion devices.[41] However, the massive particle reorganization induced through this complex reaction is still badly understood and can easily lead to pulverization and loss of electrical contact. At the electrode/electrolyte interface, the SEI forms by reduction of solvents at potentials close to those already identified for graphite electrodes. In the case of $NiSb_2$, the conversion reaction results in the formation of new "fresh" surfaces (Li_3Sb and Ni nanograins) which generate additional electrolyte consumption and the continuous creation of a growing SEI layer. Thanks to operando FTIR spectroscopy, the Li^+ dynamics at the electrode/electrolyte interface can be followed in detail during electrochemical cycling in a working cell and bring precious information on the mechanism of the electrochemical system. IR spectra recorded along the discharge/charge of the $NiSb_2$/Li electrochemical system have shown to be an accurate tool to follow the solvation of Li^+ by solvent or electrolyte degradation species and indirectly the reaction of lithiation/delithiation of this active material. The operando following of the solvation/desolvation of Li^+ during electrochemical cycling confirms (i) the phase separation occurring for conversion materials and (ii) the nanostructuration of the electrode during the first discharge since only limited changes are observed upon the following cycles. Further studies will be carried out to gather additional information related to the kinetic of the Li^+-containing species upon cycling or during relaxation (when no electrochemical reaction is expected).

DOI: 10.1021/acs.jpcc.7b06685
J. Phys. Chem. C 2017, 121, 26598−26606

■ ASSOCIATED CONTENT

Supporting Information

The Supporting Information is available free of charge on the ACS Publications website at DOI: 10.1021/acs.jpcc.7b06685.

Operando IR spectra during the 1st charge and discharge of $NiSb_2$ electrode cycled at 1C rate with 1 M $LiPF_6$ in EC:DMC (1:1) + 2%$_{vol}$ VC electrolyte. The cumulated acoustic emission energy (CAEE) during the 1st discharge of $NiSb_2$ electrode compared to the galvnostatic curve. Evolution of the peak position and voltage profile versus time during the electrochemical cycling for the bands of DMC and EC. Examples of the evolution of the IR bands related to DMC during the first discharge of $NiSb_2$. (PDF)

■ AUTHOR INFORMATION

Corresponding Author

*E-mail: laure.monconduit@umontpellier.fr.

ORCID

Nicolas Louvain: 0000-0001-8727-6832

Laure Monconduit: 0000-0003-3698-856X

Notes

The authors declare no competing financial interest.

■ ACKNOWLEDGMENTS

Alistore-European Research Institute and ADEME are gratefully acknowledged for their financial support through the postdoc grant to A.B. and the Ph.D. grant to C.M., respectively. This research was performed in the framework of the ANR Program No. ANR-11BS09-009-01.

■ REFERENCES

(1) Tarascon, J.-M.; Armand, M. Issues and Challenges Facing Rechargeable Lithium Batteries. *Nature* **2001**, *414*, 359−367.

(2) Li, J.-T.; Zhou, Z.-Y.; Broadwell, I.; Sun, S. In-Situ Infrared Spectroscopic Studies of Electrochemical Energy Conversion and Storage. *Acc. Chem. Res.* **2012**, *45*, 485−494.

(3) Peled, E. The Electrochemical Behavior of Alkali and Alkaline Earth Metals in Nonaqueous Battery Systems—The Solid Electrolyte Interphase Model. *J. Electrochem. Soc.* **1979**, *126*, 2047−2051.

(4) Balbuena, P. B.; Wang, Y. *Lithium-Ion Batteries - Solid-Electrolyte Interphase*; Balbuena, P. B., Wang, Y., Eds.; Imperial College Press: London, 2004.

(5) Smith, A. J.; Burns, J. C.; Trussler, S.; Dahn, J. R. Precision Measurements of the Coulombic Efficiency of Lithium-Ion Batteries and of Electrode Materials for Lithium-Ion Batteries. *J. Electrochem. Soc.* **2010**, *157*, A196−A202.

(6) Shim, J.; Kostecki, R.; Richardson, T. J.; Song, X.; Striebel, K. A. Electrochemical Analysis for Cycle Performance and Capacity Fading of a Lithium-Ion Battery Cycled at Elevated Temperature. *J. Power Sources* **2002**, *112*, 222−230.

(7) Menkin, S.; Golodnitsky, D.; Peled, E. Artificial Solid-Electrolyte Interphase (SEI) for Improved Cycleability and Safety of Lithium−ion Cells for EV Applications. *Electrochem. Commun.* **2009**, *11*, 1789−1791.

(8) Gu, M.; Parent, L. R.; Mehdi, B. L.; Unocic, R. R.; McDowell, M. T.; Sacci, R. L.; Xu, W.; Connell, J. G.; Xu, P.; Abellan, P.; et al. Demonstration of an Electrochemical Liquid Cell for Operando Transmission Electron Microscopy Observation of the Lithiation/Delithiation Behavior of Si Nanowire Battery Anodes. *Nano Lett.* **2013**, *13*, 6106−6112.

(9) Williamson, M. J.; Tromp, R. M.; Vereecken, P. M.; Hull, R.; Ross, F. M. Dynamic Microscopy of Nanoscale Cluster Growth at the Solid-Liquid Interface. *Nat. Mater.* **2003**, *2*, 532−536.

(10) White, E. R.; Singer, S. B.; Augustyn, V.; Hubbard, W. A.; Mecklenburg, M.; Dunn, B.; Regan, B. C. In Situ Transmission Electron Microscopy of Lead Dendrites and Lead Ions in Aqueous Solution. *ACS Nano* **2012**, *6*, 6308−6317.

(11) Ogata, K.; Salager, E.; Kerr, C. J.; Fraser, A. E.; Ducati, C.; Morris, A. J.; Hofmann, S.; Grey, C. P. Revealing Lithium−silicide Phase Transformations in Nano-Structured Silicon-Based Lithium Ion Batteries via in Situ NMR Spectroscopy. *Nat. Commun.* **2014**, *5*, 3217.

(12) Key, B.; Bhattacharyya, R.; Morcrette, M.; Seznec, V.; Tarascon, J.-M.; Grey, C. P. Real-Time NMR Investigations of Structural Changes in Silicon Electrodes for Lithium-Ion Batteries. *J. Am. Chem. Soc.* **2009**, *131*, 9239−9249.

(13) Liu, X.; Wang, D.; Liu, G.; Srinivasan, V.; Liu, Z.; Hussain, Z.; Yang, W. Distinct Charge Dynamics in Battery Electrodes Revealed by in Situ and Operando Soft X-Ray Spectroscopy. *Nat. Commun.* **2013**, *4*, 2568.

(14) Leriche, J.-B.; Hamelet, S.; Shu, J.; Morcrette, M.; Masquelier, C.; Ouvrard, G.; Zerrouki, M.; Soudan, P.; Belin, S.; Elkaïm, E.; et al. An Electrochemical Cell for Operando Study of Lithium Batteries Using Synchrotron Radiation. *J. Electrochem. Soc.* **2010**, *157*, A606.

(15) Inaba, M.; Yoshida, H.; Ogumi, Z.; Abe, T.; Mizutani, Y.; Asano, M. In Situ Raman Study on Electrochemical Li Intercalation into Graphite. *J. Electrochem. Soc.* **1995**, *142*, 20.

(16) Chen, D.; Xiong, X.; Zhao, B.; Mahmoud, M. A.; El-Sayed, M. A.; Liu, M. Probing Structural Evolution and Charge Storage Mechanism of NiO2H X Electrode Materials Using In Operando Resonance Raman Spectroscopy. *Adv. Sci.* **2016**, *3*, 1500433.

(17) Joho, F.; Novák, P. SNIFTIRS Investigation of the Oxidative Decomposition of Organic-Carbonate-Based Electrolytes for Lithium-Ion Cells. *Electrochim. Acta* **2000**, *45*, 3589−3599.

(18) Burba, C. M.; Frech, R. In Situ Transmission FTIR Spectroelectrochemistry: A New Technique for Studying Lithium Batteries. *Electrochim. Acta* **2006**, *52*, 780−785.

(19) Bewick, A.; Kunimatsu, K.; Stanley Pons, B. Infra Red Spectroscopy of the Electrode-Electrolyte Interphase. *Electrochim. Acta* **1980**, *25*, 465−468.

(20) Pons, S. The Use of Fourier Transform Infrared Spectroscopy for in Situ Recording of Species in the Electrode-Electrolyte Solution Interphase. *J. Electroanal. Chem. Interfacial Electrochem.* **1983**, *150*, 495−504.

(21) Li, J.-T.; Chen, S.-R.; Fan, X.-Y.; Huang, L.; Sun, S.-G. Studies of the Interfacial Properties of an Electroplated Sn Thin Film Electrode/electrolyte Using in Situ MFTIRS and EQCM. *Langmuir* **2007**, *23*, 13174−13180.

(22) Li, J.-T.; Chen, S.-R.; Ke, F.-S.; Wei, G.-Z.; Huang, L.; Sun, S.-G. In Situ Microscope FTIR Spectroscopic Studies of Interfacial Reactions of Sn−Co Alloy Film Anode of Lithium Ion Battery. *J. Electroanal. Chem.* **2010**, *649*, 171−176.

(23) Alves Dalla Corte, D.; Caillon, G.; Jordy, C.; Chazalviel, J.-N.; Rosso, M.; Ozanam, F. Spectroscopic Insight into Li-Ion Batteries during Operation: An Alternative Infrared Approach. *Adv. Energy Mater.* **2016**, *6*, 1501768.

(24) Yang, J.; Solomatin, N.; Kraytsberg, A.; Ein-Eli, Y. In-Situ Spectro-Electrochemical Insight Revealing Distinctive Silicon Anode Solid Electrolyte Interphase Formation in a Lithium-Ion Battery. *Chem. Sel.* **2016**, *1*, 572−576.

(25) Hongyou, K.; Hattori, T.; Nagai, Y.; Tanaka, T.; Nii, H.; Shoda, K. Dynamic in Situ Fourier Transform Infrared Measurements of Chemical Bonds of Electrolyte Solvents during the Initial Charging Process in a Li Ion Battery. *J. Power Sources* **2013**, *243*, 72−77.

(26) Zhang, X.; Kostecki, R.; Richardson, T. J.; Pugh, J. K.; Ross, P. N. Electrochemical and Infrared Studies of the Reduction of Organic Carbonates. *J. Electrochem. Soc.* **2001**, *148*, A1341−A1345.

(27) Pérez-Villar, S.; Lanz, P.; Schneider, H.; Novák, P. Characterization of a Model Solid Electrolyte Interphase/carbon Interface by Combined in Situ Raman/Fourier Transform Infrared Microscopy. *Electrochim. Acta* **2013**, *106*, 506−515.

(28) Zhuang, G. V.; Ross, P. N. Analysis of the Chemical Composition of the Passive Film on Li-Ion Battery Anodes Using

DOI: 10.1021/acs.jpcc.7b06685
J. Phys. Chem. C 2017, 121, 26598−26606

Attenuated Total Reflection Infrared Spectroscopy. *Electrochem. Solid-State Lett.* **2003**, *6*, A136−A139.
(29) Aurbach, D.; Moshkovich, M.; Cohen, Y.; Schechter, A. The Study of Surface Film Formation on Noble-Metal Electrodes in Alkyl Carbonates/Li Salt Solutions, Using Simultaneous in Situ AFM, EQCM, FTIR, and EIS. *Langmuir* **1999**, *15*, 2947−2960.
(30) Aurbach, D.; Daroux, M.; Faguy, P.; Yeager, E. The Electrochemistry of Noble Metal Electrodes in Aprotic Organic Solvents Containing Lithium Salts. *J. Electroanal. Chem. Interfacial Electrochem.* **1991**, *297*, 225−244.
(31) Bridel, J.-S.; Grugeon, S.; Laruelle, S.; Hassoun, J.; Reale, P.; Scrosati, B.; Tarascon, J.-M. Decomposition of Ethylene Carbonate on Electrodeposited Metal Thin Film Anode. *J. Power Sources* **2010**, *195*, 2036−2043.
(32) Yang, H.; Zhuang, G. V.; Ross, P. N. Thermal Stability of LiPF6 Salt and Li-Ion Battery Electrolytes Containing LiPF6. *J. Power Sources* **2006**, *161*, 573−579.
(33) Campion, C. L.; Li, W.; Lucht, B. L. Thermal Decomposition of LiPF6-Based Electrolytes for Lithium-Ion Batteries. *J. Electrochem. Soc.* **2005**, *152*, A2327−A2334.
(34) Borodin, O.; Olguin, M.; Ganesh, P.; Kent, P. R. C.; Allen, J. L.; Henderson, W. A. Competitive Lithium Solvation of Linear and Cyclic Carbonates from Quantum Chemistry. *Phys. Chem. Chem. Phys.* **2016**, *18*, 164−175.
(35) Cui, W.; Lansac, Y.; Lee, H.; Hong, S.-T.; Jang, Y. H. Lithium Ion Solvation by Ethylene Carbonates in Lithium-Ion Battery Electrolytes, Revisited by Density Functional Theory with the Hybrid Solvation Model and Free Energy Correction in Solution. *Phys. Chem. Chem. Phys.* **2016**, *18*, 23607−23612.
(36) Seo, D. M.; Reininger, S.; Kutcher, M.; Redmond, K.; Euler, W. B.; Lucht, B. L. Role of Mixed Solvation and Ion Pairing in the Solution Structure of Lithium Ion Battery Electrolytes. *J. Phys. Chem. C* **2015**, *119*, 14038−14046.
(37) Chapman, N.; Borodin, O.; Yoon, T.; Nguyen, C. C.; Lucht, B. L. Spectroscopic and Density Functional Theory Characterization of Common Lithium Salt Solvates in Carbonate Electrolytes for Lithium Batteries. *J. Phys. Chem. C* **2017**, *121*, 2135−2148.
(38) Masia, M.; Probst, M.; Rey, R. Ethylene Carbonate−Li+: A Theoretical Study of Structural and Vibrational Properties in Gas and Liquid Phases. *J. Phys. Chem. B* **2004**, *108*, 2016−2027.
(39) Brooksby, P. A.; Fawcett, W. R. Infrared (Attenuated Total Reflection) Study of Propylene Carbonate Solutions Containing Lithium and Sodium Perchlorate. *Spectrochim. Acta, Part A* **2006**, *64*, 372−382.
(40) Fulfer, K. D.; Kuroda, D. G. Solvation Structure and Dynamics of the Lithium Ion in Organic Carbonate-Based Electrolytes: A Time-Dependent Infrared Spectroscopy Study. *J. Phys. Chem. C* **2016**, *120*, 24011−24022.
(41) Cabana, J.; Monconduit, L.; Larcher, D.; Palacín, M. R. Beyond Intercalation-Based Li-Ion Batteries: The State of the Art and Challenges of Electrode Materials Reacting Through Conversion Reactions. *Adv. Mater.* **2010**, *22*, E170−E192.
(42) Villevieille, C.; Ionica-Bousquet, C. M.; Ducourant, B.; Jumas, J.-C.; Monconduit, L. NiSb2 as Negative Electrode for Li-Ion Batteries: An Original Conversion Reaction. *J. Power Sources* **2007**, *172*, 388−394.
(43) Villevieille, C.; Ionica-Bousquet, C. M.; Jumas, J.-C.; Monconduit, L. 121Sb Mössbauer Study of the Electrochemical Reaction of NiSb2 vs Lithium. *Hyperfine Interact.* **2008**, *187*, 71−79.
(44) Marino, C.; Fraisse, B.; Womes, M.; Villevieille, C.; Monconduit, L.; Stievano, L. At the Heart of a Conversion Reaction: An Operando X-Ray Absorption Spectroscopy Investigation of NiSb2, a Negative Electrode Material for Li-Ion Batteries. *J. Phys. Chem. C* **2014**, *118*, 27772−27780.
(45) Marino, C.; Fullenwarth, J.; Monconduit, L.; Lestriez, B. Diagnostic of the Failure Mechanism in NiSb2 Electrode for Li Battery through Analysis of Its Polarization on Galvanostatic Cycling. *Electrochim. Acta* **2012**, *78*, 177−182.
(46) Loring, J. S.; Fawcett, W. R. Ion−Solvent Interactions in Acetonitrile Solutions of Lithium, Sodium, and Tetraethylammonium Perchlorate Using Attenuated Total Reflectance FTIR Spectroscopy. *J. Phys. Chem. A* **1999**, *103*, 3608−3617.
(47) Barthel, J.; Buchner, R.; Wismeth, E. FTIR Spectroscopy of Ion Solvation of LiClO4 and LiSCN in Acetonitrile, Benzonitrile, and Propylene Carbonate. *J. Solution Chem.* **2000**, *29*, 937−954.
(48) Aurbach, D.; Gamolsky, K.; Markovsky, B.; Gofer, Y.; Schmidt, M.; Heider, U. On the Use of Vinylene Carbonate (VC) as an Additive to Electrolyte Solutions for Li-Ion Batteries. *Electrochim. Acta* **2002**, *47*, 1423−1439.
(49) Aroca, R.; Nazri, M.; Nazri, G. A.; Camargo, A. J.; Trsic, M. Vibrational Spectra and Ion-Pair Properties of Lithium Hexafluorophosphate in Ethylene Carbonate Based Mixed-Solvent Systems for Lithium Batteries. *J. Solution Chem.* **2000**, *29*, 1047−1060.
(50) Ikezawa, Y.; Nishi, H. In Situ FTIR Study of the Cu Electrode/ethylene Carbonate+dimethyl Carbonate Solution Interface. *Electrochim. Acta* **2008**, *53*, 3663−3669.
(51) Fortunato, B.; Mirone, P.; Fini, G. Infrared and Raman Spectra and Vibrational Assignment of Ethylene Carbonate. *Spectrochim. Acta A Mol. Biomol. Spectrosc.* **1971**, *27*, 1917−1927.
(52) Durig, J. R.; Clark, J. W.; Casper, J. M. Vibrational Spectra and Structure of Small Ring Compounds XVII. Far Infrared and Matrix Spectra of Vinylene Carbonate. *J. Mol. Struct.* **1970**, *5*, 67−84.
(53) Peng, Q.; Liu, H.; Ye, S. Adsorption of Organic Carbonate Solvents on a Carbon Surface Probed by Sum Frequency Generation (SFG) Vibrational Spectroscopy. *J. Electroanal. Chem.* **2017**, *800*, 134−143.
(54) Villevieille, C.; Boinet, M.; Monconduit, L. Direct Evidence of Morphological Changes in Conversion Type Electrodes in Li-Ion Battery by Acoustic Emission. *Electrochem. Commun.* **2010**, *12*, 1336−1339.
(55) Matsuoka, O.; Hiwara, A.; Omi, T.; Toriida, M.; Hayashi, T.; Tanaka, C.; Saito, Y.; Ishida, T.; Tan, H.; Ono, S. S.; et al. Ultra-Thin Passivating Film Induced by Vinylene Carbonate on Highly Oriented Pyrolytic Graphite Negative Electrode in Lithium-Ion Cell. *J. Power Sources* **2002**, *108*, 128−138.
(56) Yoshida, H.; Fukunaga, T.; Hazama, T.; Terasaki, M.; Mizutani, M.; Yamachi, M. Degradation Mechanism of Alkyl Carbonate Solvents Used in Lithium-Ion Cells during Initial Charging. *J. Power Sources* **1997**, *68*, 311−315.
(57) Verma, P.; Maire, P.; Novák, P. A Review of the Features and Analyses of the Solid Electrolyte Interphase in Li-Ion Batteries. *Electrochim. Acta* **2010**, *55*, 6332−6341.
(58) Tasaki, K.; Goldberg, A.; Lian, J.-J.; Walker, M.; Timmons, A.; Harris, S. J. Solubility of Lithium Salts Formed on the Lithium-Ion Battery Negative Electrode Surface in Organic Solvents. *J. Electrochem. Soc.* **2009**, *156*, A1019−A1027.
(59) Jamnik, J.; Maier, J. Nanocrystallinity Effects in Lithium Battery Materials. *Phys. Chem. Chem. Phys.* **2003**, *5*, 5215−5220.
(60) Gachot, G.; Grugeon, S.; Armand, M.; Pilard, S.; Guenot, P.; Tarascon, J.-M.; Laruelle, S. Deciphering the Multi-Step Degradation Mechanisms of Carbonate-Based Electrolyte in Li Batteries. *J. Power Sources* **2008**, *178*, 409−421.
(61) Zhang, W.; Ghamouss, F.; Darwiche, A.; Monconduit, L.; Lemordant, D.; Dedryvère, R.; Martinez, H. Surface Film Formation on TiSnSb Electrodes: Impact of Electrolyte Additives. *J. Power Sources* **2014**, *268*, 645−657.
(62) Marino, C.; Sougrati, M. T.; Gerke, B.; Pöttgen, R.; Huo, H.; Ménétrier, M.; Grey, C. P.; Monconduit, L. Role of Structure and Interfaces in the Performance of TiSnSb as an Electrode for Li-Ion Batteries. *Chem. Mater.* **2012**, *24*, 4735−4743.

DOI: 10.1021/acs.jpcc.7b06685
J. Phys. Chem. C 2017, 121, 26598−26606